HYDRODYNAMIC PREDICTION OF THE DUCTED PROPELLER BY CFD SOLVER

Sohrab Majdfar
Department of mechanical engineering, Imam Khomeini Naval University, Nowshahr, Iran.

Hassan Ghassemi
Department of Maritime Engineering, AmirKabir University of Technology, Tehran, Iran., gasemi@aut.ac.ir

Hamid Forouzan
Department of mechanical engineering, Imam Khomeini Naval University, Nowshahr, Iran.

Arash Ashrafi
Department of Maritime Engineering, AmirKabir University of Technology, Tehran, Iran.

HYDRODYNAMIC PREDICTION OF THE DUCTED PROPELLER BY CFD SOLVER

Acknowledgements

HYDRODYNAMIC PREDICTION OF THE DUCTED PROPELLER BY CFD SOLVER

Sohrab Majdfar[2], Hassan Ghassemi[1], Hamid Forouzan[2], and Arash Ashrafi[1]

ABSTRACT

Ducted propellers are usually used in many kinds of vessels, i.e., fishing vessels, trawlers, and submarines which have provided high efficiency in propulsion system. In this article, the effects of the length and angle of 19A type duct on the hydrodynamic performance were investigated. First, the ducted propeller (19A type duct) was selected for the study and modeling of this duct was later developed. Then, ducted propeller performance was analyzed by a RANS turbulence model of SST-K-ω and validated with the experimental results which indicated an acceptable accuracy. Finally, the effects of the implemented changes were analyzed considering the alternation of the angle of the duct and the duct size at a rate of 10 and 20 percent of the original length. In this regard, Numerical results included pressure distribution, hydrodynamic characteristics and velocity behind the propeller of various geometries and physical conditions. The effects of the duct angle and propeller location were presented and discussed, as well.

I. INTRODUCTION

Ducted propellers are comprised of an annular duct and a propeller. There are two types of duct, i.e., accelerating and decelerating ones. Although the accelerating ducted propeller is mostly used for the ships, the decelerating duct is sometimes employed as a pump-jet system in special marine vehicles such as torpedo (Suryanarayana et al., 2014). The propeller type in this system is a Kaplan propeller with a wide blade at the tip.

The ability to accurately predict the thrust and torque of a ducted propeller in open-water conditions is very important for the calculation method used in the design stage. The Reynolds Average Navier-Stokes (RANS) methods have progressively been introduced for the calculation of ducted propeller systems leading to considerable success in predicting open-water characteristics for well-known Ka-series (Sanchez-Caja et al., 2000; Abdel-Maksoud et al., 2003; Krasilnikov et al., 2007; and Abdel-Makoud et al., 2010). Moreover, calculation of the propeller noise was predicted by Takinaci and Taralp (2013). However, due to its relative complexity and time requirement, it is not yet routinely used in the design process which is often based on the use of inviscid flow methods. Krasilnikov studied mesh generation techniques for the analysis of ducted propellers using a commercial RANS solver and its application to scale effect.

Various numerical methods have been proposed based on potential flow theory for the analysis of ducted propellers. For example, combination of a panel method which is also known as Boundary Element Method (BEM) with a vortex lattice method was utilized in order to model the duct for the propeller (Kerwin et al., 1987).

A type of panel method for the complete ducted propeller system operating in unsteady flow conditions including blade sheet cavitation was presented by Lee et al. (2006). Both methods applied a transpiration velocity model for the gap flow between propeller blade tip and duct inner surface, as well as analyzed duct with a sharp trailing edge. It was indicated that although the use of non-viscous flow model for ducted propellers is beneficial, there may be some serious limitations in the areas of flow where viscosity effects cannot be ignored and should be modeled for the correct prediction of thrust and torque of ducted propeller. One of such regions is related to the gap flow, which has a strong impact not only on the propeller and duct circulation distribution, but also on the distribution of loading between propeller and duct (Baltazar et al., 2009; 2011). In addition, there may be considerable interaction between the vortices shed from the propeller blade tips and the boundary layer developing on the duct inner side (Rijpkema et al., 2011). This effect has not been previously taken into account with potential flow methods.

Nevertheless, a design for ducted propellers and model tests of a research fishing vessel for M. Cies Shipyards were presented (Bobo et al., 2005). A specific technique of modeling between the inner plate of duct and propeller tip was also studied by Hughes (1997) and Moon et al. (2002). Moreover, a research work on calculation of ducted propeller performance in axisymmetric flows was carried out by Falco et al. (1983). An RANS analysis tool for ducted propeller systems in open water con-

ditions was presented (Hoekstra, 2006). The flow analysis, design and model testing of ducted propellers were reported by Zondervan et al. (2006). The flow around a ducted propeller by a vortex lattice and finite volume methods was investigated by Gu et al. (2003). Also, Haimov et al. (2010) conducted a research work on ducted propellers as better propulsion of ship by calculations and practices. An experimental and numerical study on wake vortex noise of a low speed propeller fan was also carried out by Sasaki et al. (2012). A series of works based on both potential method and RANS solver for the whole geometry have been performed for a multi-component linear jet optimization (Steden et al., 2009). The hydrodynamic performances of different rudders were analyzed using a CFD approach. Meanwhile, a three-dimensional turbulent flow around rudders has been computed via solving the RANS equations combined with the $k - \varepsilon$ turbulent model (Chau et al., 2005).

In the present study, the CFD commercial software (ANSYS-CFX) was employed to predict the hydrodynamic performance of the ducted propeller. The effect of the position of the propeller inside duct and the duct angle was investigated. The numerical results of the pressure distribution, hydrodynamic characteristics, and flow field in the propeller downstream were also presented and discussed.

II. GOVERNING EQUATIONS

The three-dimensional flow of incompressible viscous fluid can be described via continuity equation and three equations of motion in the direction of the Cartesian coordinates called Navier-Stokes equations.

1. Continuity Equation

The basic law of fluid mechanics, the law of conservation of mass that was expressed by Euler, is as follows:

$$\frac{\partial \rho}{\partial t} + \nabla \cdot (\rho \boldsymbol{U}) = 0 \tag{1}$$

For the incompressible fluid $\left(D\rho / Dt = 0 \right)$, Eq. (1) can be converted as:

$$\nabla \cdot \boldsymbol{U} = 0 \tag{2}$$

2. Momentum Conservation Equation

Newton's second law states that the rate of change in mass momentum of the fluid is equal to the net external force acting on the mass. Therefore, the equation of momentum conservation is expressed as:

$$\rho \frac{D\boldsymbol{U}}{Dt} = \boldsymbol{f}_s + \boldsymbol{f}_b \tag{3}$$

where f_s is surface forces and f_b is body forces. Here, the volume forces are equal to gravity. Also the surface forces acting on fluid were brought about by tensions viscosity (shear stress) and

the fluid pressure. Thus, Eq. (3) is expressed as follows:

$$\rho \frac{Du_i}{Dt} = \frac{\partial \tau_{ij}}{\partial x_j} + \rho G_i \tag{4}$$

where τ_{ij} includes the vertical and shear stresses. If $i = j$, the stress is normal stress and in other cases the stress is shear stress.

In order to solve the fluid flow, continuity equation should be written as well as the momentum equations. So, there are 10 unknowns and 4 equations which can't be solved. For solving the equations, some other equations are required. According to shear stress law, the ratio of the fluid deformation rate and the shear stress are linearly dependent on the fluid viscosity:

$$\tau_{xy} = \mu \gamma_{xy} = \mu \left(\frac{\partial u}{\partial y} + \frac{\partial v}{\partial x} \right)$$
$$\tau_{yz} = \mu \gamma_{yz} = \mu \left(\frac{\partial v}{\partial z} + \frac{\partial w}{\partial y} \right) \tag{5}$$
$$\tau_{xz} = \mu \gamma_{xz} = \mu \left(\frac{\partial u}{\partial z} + \frac{\partial w}{\partial x} \right)$$

Also, it is assumed that normal stresses also have linear relations with the deformation rate and the Eq. (6) relations are achieved:

$$\sigma_{xx} = -P + 2\mu \frac{\partial u}{\partial x} + \frac{2}{3} \mu \nabla \cdot \boldsymbol{U}$$
$$\sigma_{yy} = -P + 2\mu \frac{\partial v}{\partial y} + \frac{2}{3} \mu \nabla \cdot \boldsymbol{U} \tag{6}$$
$$\sigma_{zz} = -P + 2\mu \frac{\partial w}{\partial z} + \frac{2}{3} \mu \nabla \cdot \boldsymbol{U}$$

Using Eq. (4) and assuming an incompressible fluid, the Navier-Stokes equations are defined as follows:

$$\frac{\partial \boldsymbol{U}}{\partial t} + \boldsymbol{U} \cdot \nabla \boldsymbol{U} = -\frac{1}{\rho} \nabla (P + \rho g z) + \nu \nabla^2 \boldsymbol{U} \tag{7}$$

For steady flow $\left(\partial \boldsymbol{U} / \partial t = 0 \right)$, Eq. (7) is defined as:

$$\boldsymbol{U} \cdot \nabla \boldsymbol{U} = -\frac{1}{\rho} \nabla (P + \rho g z) + \nu \nabla^2 \boldsymbol{U} \tag{8}$$

The preceding set of equations represents four equations that can be satisfied by the four unknowns. The continuity equation (Eq. (2)) supplies one scalar equation, while the Navier-Stokes equation (Eq. (7)) supplies three scalar equations. The four unknowns are pressure P, and velocity $U = (u, v, w)$. The parameters of ρ and ν are defined as constants.

III. GEOMETRIC MODELING

The most common propeller in ducted propellers is Kaplan.

Table 1. Duct characteristics and geometric parameters.

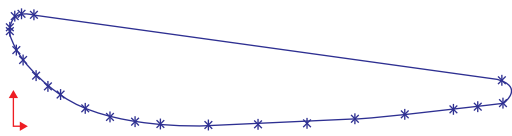| Parameter	Value
Propeller Dia.	D_p = 300 mm
Number of blades	Z=4
Pitch-diameter ratio	P/D = 0.8
Expanded Area Ratio	EAR = 0.70
Duct length	L = 0.5 D_P
Gap at tip	0.01 D_p
Propeller type	Kaplan (Ka)
Duct type	19A

Fig. 1. Section of 19A duct.

The Ka4-70 (means number of blade (Z) which is 4 and expanded area ratio (EAR) is 0.70) propeller comes from the famous Wageningen propeller series. So, it is a traditional ducted propeller that has a large chord at the tip. The ducted propeller with a Pitch/Diameter (P/D) ratio of 0.8 was used in all the results achieved in this paper. The propeller and its duct were both modeled by Propcad and Solidworks software. Ducted propeller geometrical data is also shown in Table 1.

Furthermore, the 19A and 37 duct types are the most common types of duct due to the favorable hydrodynamic properties. Being an accelerator duct, 19A duct type was applied in this paper. The duct length was equal to half of the propeller diameter and the distance between the propeller tip and the inner surface of the duct was equal to one percent of the propeller diameter (3 mm). Fig. 1 shows the section of the 19A duct. Also, a three-dimensional model of the ducted propeller and the assembled ducted propeller are shown in Fig. 2.

IV. MESH GENERATION AND BOUNDARY CONDITIONS

After modeling ducted propeller and domain, they were divided into 4 pieces and one piece was applied to the smaller cells for achieving a higher accuracy in calculations. The computational domain basically consisted of an internal rotating cylinder containing the propeller and an external stationary cylinder with radius 1.5D. On the other hand, the inlet uniform boundary condition was located at 3D upstream of the propeller plane and the constant pressure condition was imposed 6.5D downstream shown in Fig. 3. At the inlet and outlet of the cylinder the velocity and pressure were prescribed respectively. For a thrust producing operating condition in the propeller, the fluid which went through the duct was accelerated. Then, ICEM meshing tools were applied.

In this analysis, the rotational velocity of the propeller was imposed by a Moving Reference Frame (MRF) applied to the

(a)
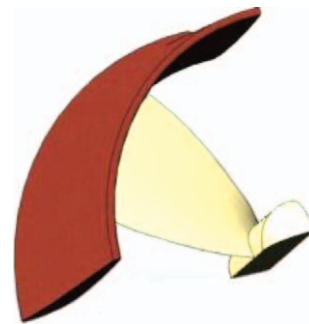
(b)

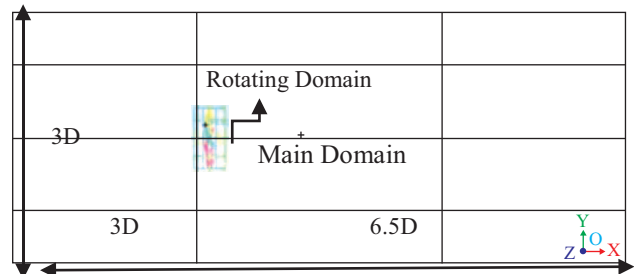**Fig. 2. (a) 3D model of ducted propeller and (b) Assembled of ducted propeller.**

Fig. 3. Computational domains dimensions.

inner region of the domain due to low time in computation and acceptable accuracy in simulation. All domains were divided into two sections:

(1) main domain that was stationary domain with larger mesh; and

(2) rotating domain with small mesh around propeller that is shown in Fig. 4.

The generated mesh size was increased outward with the ratio of 1.2 and then it defined boundary conditions including inlet, outlet, rotating domain, open water, propeller, and duct. Fig. 5 shows the meshes near propeller and duct. First, a mesh with 1 million cells was used as a model, and then smaller mesh with 1.4, 1.5 and 1.7 million cells were utilized. After that the results were compared at advance coefficient of 0.4. Comparison of re-

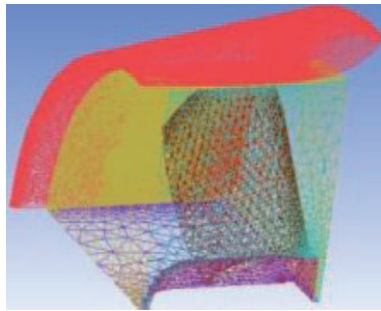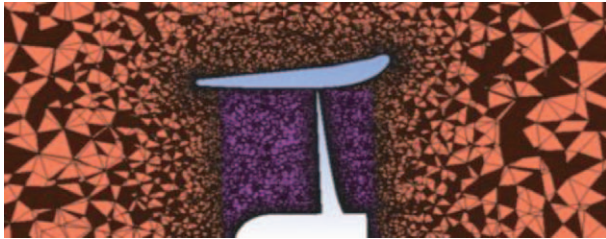**Fig. 4. Division of calculation domain with mesh.**

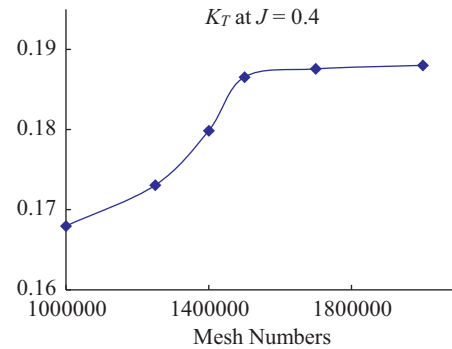**Fig. 5. Mesh cells on the propeller and duct at different views.**

Fig. 6. Result Independence from meshes.

Fig. 7. Comparison of the numerical and experimental hydrodynamics characteristics of ducted propeller.

sults indicated that the minimum number of cells for this model is 1.4 million and Fig. 6 shows the results independence from meshes.

V. SOLVER SETTINGS

The applied CFD code was ANSYS CFX v.14. The RANS equations were solved numerically by a finite volume technique. Also, High Resolution Method was used to discrete equations and first order method was applied to investigate turbulence. Moreover, Shear Stress Transport (SST) model was selected for turbulence model since it was applied in most research works due to its higher accuracy. Then, 3000 iterations were selected for determining the number of iteration to achieve convergence and the remaining amount was considered 0.0001. For accuracy in solver results, conservation target with 0.01 value was used controlling the difference between input and output.

VI. VALIDATION

After finalizing the solver module, the numerical results were compared with the experimental results to validate the software. The software outputs were thrust coefficient, torque coefficient and efficiency obtained by thrust and torque of propeller and duct. The hydrodynamic characteristics of propeller (thrust coefficient, K_T, torque coefficient, K_Q, and efficiency, η) as well as the advance coefficient (J) are defined as follows:

$$K_T = \frac{T}{\rho n^2 D^4}, K_Q = \frac{Q}{\rho n^2 D^5}$$
$$\eta = \frac{K_T}{K_Q} \cdot \frac{J}{2\pi}, J = \frac{V_A}{nD} \qquad (9)$$

where V_A is advance velocity, n is rotational velocity, D is propeller diameter, T is total thrust, ρ is water density and Q indicates total torque. A comparison of the numerical and experimental data is shown in Fig. 7. The relative error was about less than 10%. Also, the pressure contours on face and back of propeller at advance coefficient, $J = 0.3$, were shown in Fig. 8. The blade tip was located where the pressure lines converge. Also, on the suction side of the blade tip, a low pressure area can be observed.

VII. RESULTS

1. Increase in the Duct Length:

1) In the Case of 10% Increase in the Duct Length

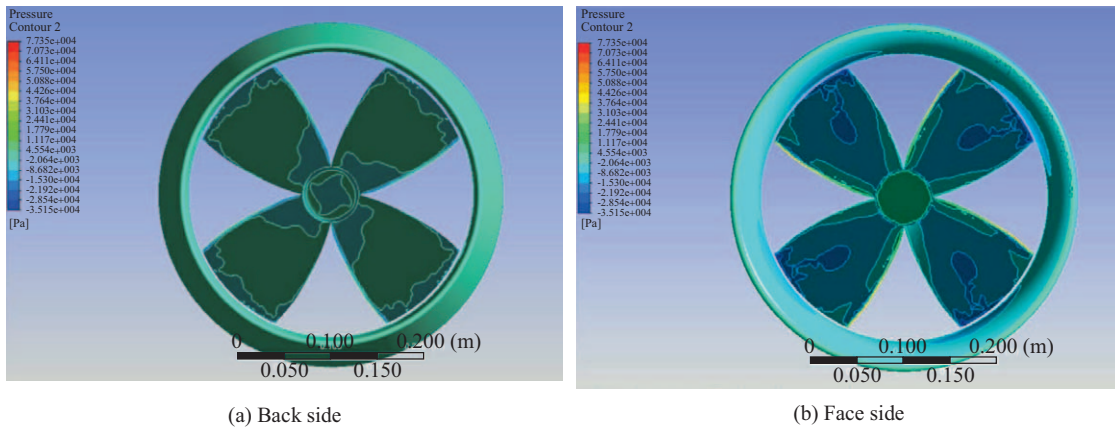The effect of duct length on the hydrodynamic characteristics

(a) Back side   (b) Face side

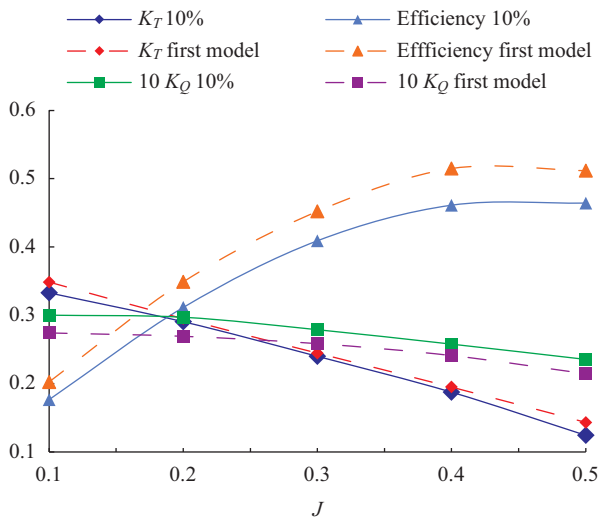**Fig. 8. Pressure contours at the back and face (J = 0.3).**

**Fig. 9.   Comparison of the hydrodynamics characteristics of ducted pro-
peller (initial duct and 10% increased duct length).**

(a) Velocity vector

(b) Velocity contour

**Fig. 10. Velocity vector and velocity contour (duct length increased 10%,
J = 0.3).**

was investigated. The 3D models of 19A type duct were ge-
nerated by increasing the length up to 10 and 20 percent. Then, it
was saved in the IGES format and imported to ICEM for mesh-
ing with the same settings as the original model. Afterwards, spe-
cifying the boundary settings of model in Ansys CFX-pre and
running the solver to export the results were conducted. To ex-
amine the effect of increasing the length of the duct, numerical
results were obtained for the first model.

Fig. 9 illustrates the comparison of ducted propeller with
10% increase in the duct length and the initial duct length. By
producing 10% increase in the duct length, the efficiency was
increased about 5% at low advance coefficient to 10% at high
advance coefficient. Also, the torque was increased in all ad-
vance coefficients while the thrust was slightly diminished.

Fig. 10 shows the velocity vector and velocity contour in case
of 10% increased duct length at J = 0.3. Higher velocity was
also obtained inside the duct.

Fig. 11 presents the pressure coefficient (C_p = P/0.5 ρV_A^2)
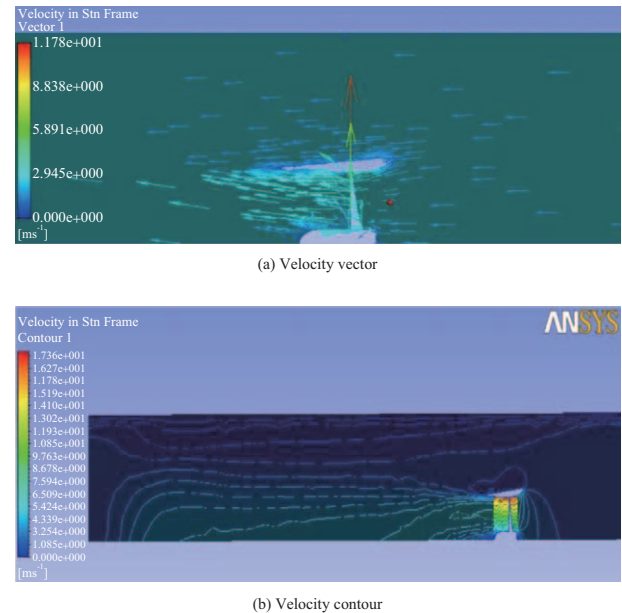on the blade at different radiuses (r/R = 0.3, 0.5 and 0.7). The

high pressure at the blade leading edge of the back side was
clearly visible. There was a cross point almost at x/c = 0.2, and
low pressure was between x/c = 0.2 and x/c = 1. At radius
r/R = 0.7, pressure region was higher than the other radius, so
much thrust can be produced at higher radius. Since the thrust
was obtained by integrating the pressure ($T = \int (\Delta p) ds$), the higher
difference in pressure results in higher thrust.

Fig. 12 depicts the pressure coefficient on duct with 10%
increase in the length. Very low pressure might be found inside
the duct and upstream of the propeller.

2) In the Case of 20% Duct Length Increase

The effect of increasing the duct length by 20% was also
investigated. The hydrodynamic characteristics of the ducted
propeller with 20% increase in the duct length were compared
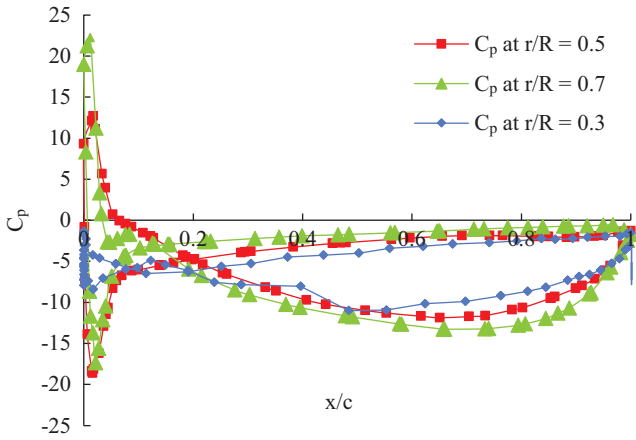in Fig. 13 which illustrates how the torque increases and effi-

Fig. 11. Pressure coefficient on propeller at different radiuses (duct length increased by 10%, *J* = 0.3).

(a) Velocity vector

(b) Velocity contour

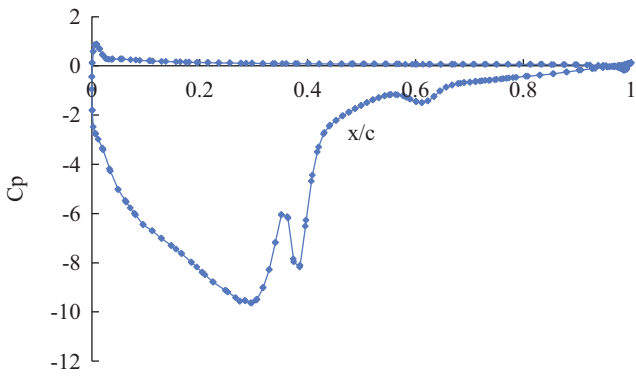**Fig. 14 Velocity distribution (duct length increased by 10%, *J* = 0.3).**

Fig. 12. Pressure distributions on duct with 10% increase in duct length (*J* = 0.3).
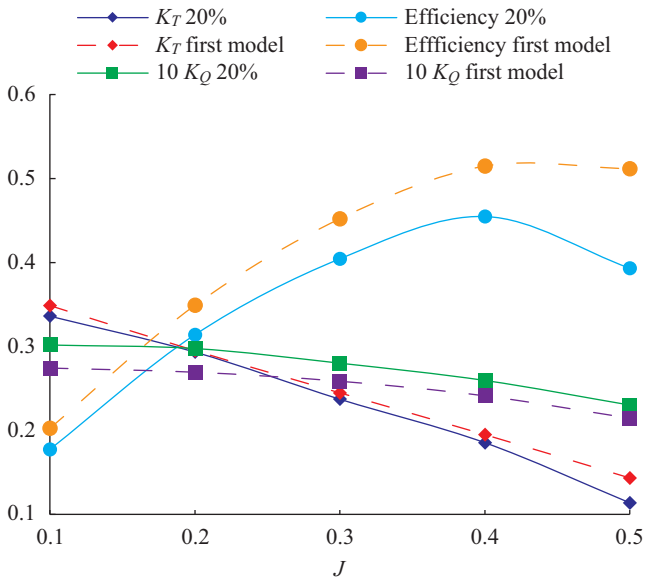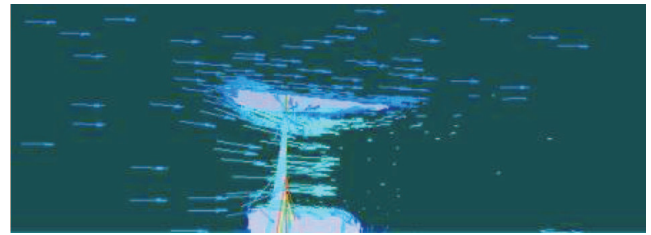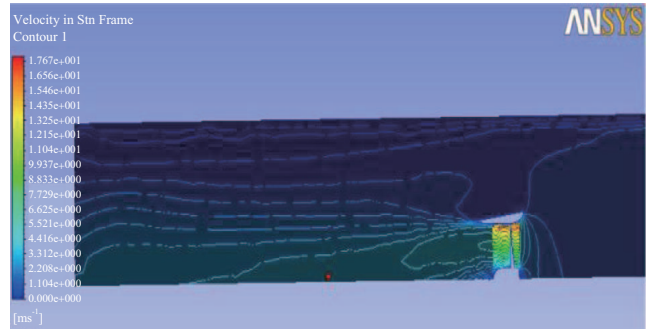

(a) 10% increase in duct length

Fig. 13. Comparison of the numerical and experimental hydrodynamics characteristics of ducted propeller.
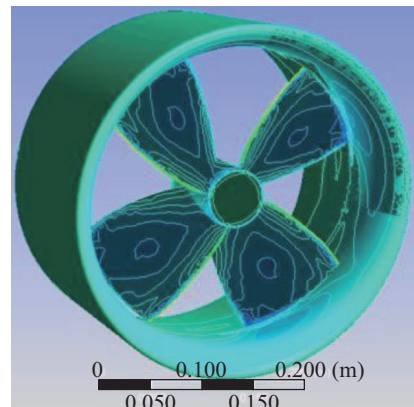
(b) 20% increase in duct length

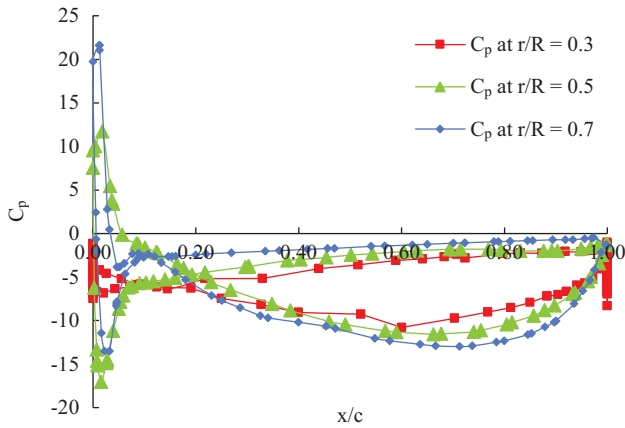**Fig. 15. Pressure distribution (*J* = 0.3).**

Fig. 16.　Pressure distributions on propeller at different radiuses in propeller with 20% increase in duct length (*J* = 0.3).
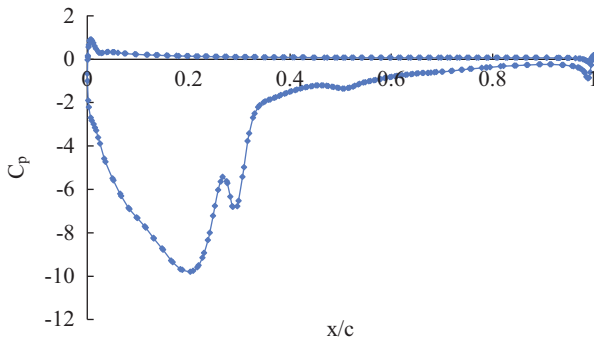

Fig. 17.　Pressure distributions on duct with 20% increase in duct length (*J* = 0.3).

ciency decreases in all advance coefficients. When duct length increased, drag increased as well, so it resulted in an increase in the torque.

Fig. 14 shows velocity vectors and contours in case of 20% increase of length at advance coefficient of 0.3 indicating decreasing in values.

Pressure contours distribution on face side of the propeller and duct at up to 10% and 20% increase in duct length is shown in Fig. 15. Moreover, Figs. 16 and 17 indicate the pressure coefficient distributions on the propeller blade (at three radius r/R = 0.3, 0.5 and 0.7) and on the duct respectively. Fig. 18 shows pressure contour on duct at 10% and 20% increase in duct length. All results of those figures were given at *J* = 0.3.

2. Increasing Duct Angle by 10 and 20 Degrees

Here, the propeller is the same as previous one but duct angle was changed by 10 and 20 degrees. Figs. 19 and 21 illustrate the hydrodynamic characteristics of the ducted propeller when the duct angle increases by 10 and 20 degrees respectively.

Fig. 20 shows the velocity vectors at duct angle = 20 degree and *J* = 0.3. Although the presentation of contour shown in some figures may not be clear for the reader, it may qualitatively give some general occurrence along the upstream and downstream of the propeller and inside the duct.
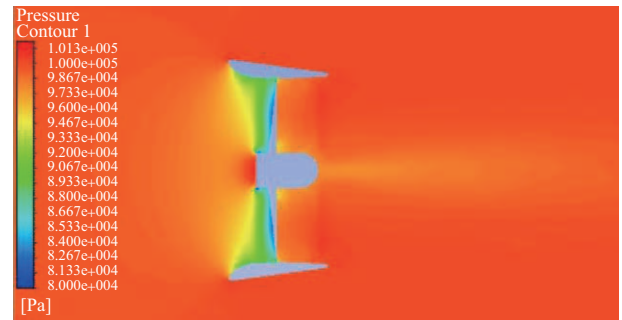
(a) 10% increase in duct length
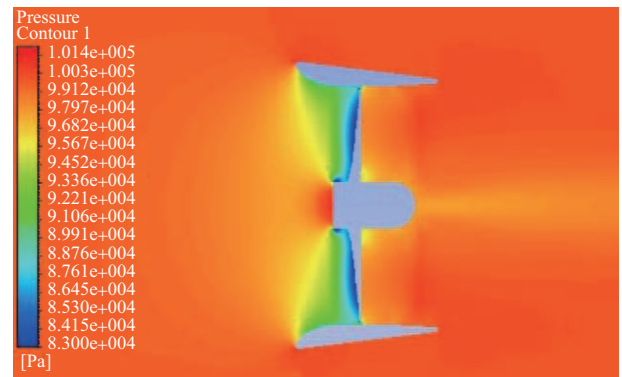
(b) 20% increase in duct length

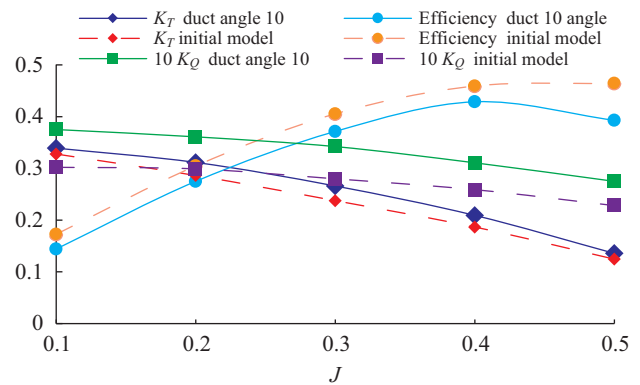**Fig. 18.　Pressure distribution (*J* = 0.3).**

Fig. 19.　Comparison of hydrodynamic characteristics of ducted propeller in case normal duct and duct with 10 degree duct angle.
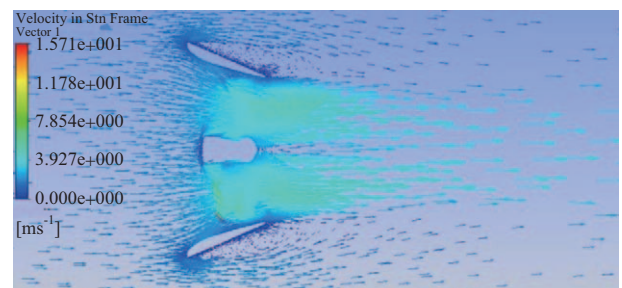

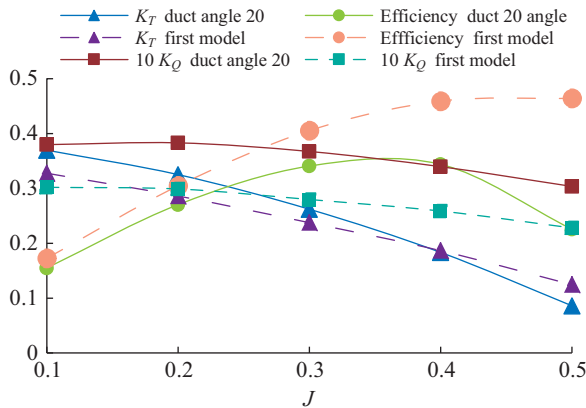**Fig. 20.　Velocity vector (duct angle = 20 deg, *J* = 0.3).**

Fig. 21. Comparison of hydrodynamic characteristics of ducted propeller in cases of normal duct and duct with 20 degree duct angle.

VIII. CONCLUSIONS

In this paper, the ducted propeller with 19A type duct was analyzed at different duct angles and duct lengths. Based on the numerical results, the following results were concluded:

(1) Pressure coefficient distribution on the duct and blade was presented in contours and diagrams. Negative low pressure coefficient was shown in back side and high pressure was given in face side of the blade. Lower pressure at suction side of the duct (inside of the duct) was also observed.

(2) Hydrodynamic characteristics of the ducted propeller were compared with experimental available data. The calculated results were found to be reasonable.

(3) In order to evaluate the effects of increasing the duct length on the performance of the propeller in open water, the duct length was increased up to 10 and 20 percent. The results showed that by increasing the duct length, both the torque and efficiency diminished while thrust coefficient did not change significantly.

(4) Effect of the duct angles proved that with increasing the duct angle, both torque and thrust were increased while efficiency decreased especially at low advance coefficient. At higher advance coefficient, thrust decreased causing the efficiency to decrease.

(5) Greater emphasis on numerical computation of different numbers and sizes of the mesh as well as other turbulent models were recommended as an alternative to the present method. Authors intend to work on the hydrodynamic performance on the wake flow (behind the ship) in near future.

ACKNOWLEDGMENTS

REFERENCES

Abdel-Maksoud, M. and H.-J. Heinke (2003). Scale effects on ducted propellers. Proc. 24th Symp. on Naval Hydrodynamics, Fukuoka, Japan.

Abdel-Maksoud, M., M. Steden and J. Hundemer (2010). Design of a multi-component propulsor. In: Proc. 28th Symposium on Naval Hydrodynamics, Pasadena, USA, September.

Baltazar J., J. A. C. Falcão de Campos and J. Bosschers (2011). Open-water thrust and torque predictions of a ducted propeller system with a panel method, 2nd Int. Symp. On Marine Propulsors SMP'11, Hamburg, Germany, June.

Baltazar, J. and J. A. C. Falcão de Campos (2009). On the modeling of the flow in ducted propellers with a panel method. Proc. of the 1st Int. Symp. on Marine Propulsors, Trondheim, Norway.

Bobo, M. J., J.-C. De La Rosa, J. Masip, R. Quereda and L. Pangusión (2005). Design of ducted propeller and model tests of a fishing research vessel for M.Cies Shipyards, OTI 2233-2, CEHIPAR. (in Spanish)

Chau, S.-W., J.-S. Kouh, T.-H. Wong and Y.-J. Chen (2005). Investigation of hydrodynamic performance of high-speed craft rudders via turbulent flow computations, Part I: non-cavitating characteristics. Journal of Marine Science and Technology 13(1), 61-72.

Falcao de Campos, J. A. C. (1983). On the calculation of ducted propeller performance in axisymmetric flows. Ph.D. Thesis, Delft University, Wageningen, the Netherlands.

Gu, H. and S. A. Kinnas (2003). Modeling of contra-rotating and ducted propellers via coupling of a vortex-lattice with a finite volume method. In: Proceedings of Propeller/Shafting Symposium, SNAME, Virginia Beach, USA.

Haimov, H., M. J. Bobo, J. Vicario and J. Del Corral (2010). Ducted propellers. A solution for better propulsion of ships.calculations and practice. Proc. of 1st Int. Symp. on Fishing Vessel Energy Efficiency, Vigo, Spain.

Hoekstra, M. (2006). A RANS-based analysis tool for ducted propeller systems in open water conditions. Int. Shipbuilding Progress 53, 205-227.

Hughes, M. J. (1997). Implementation of a special procedure for modeling the tip clearance flow in a panel method for ducted propellers. Proc. of the Propellers/Shafting'97 Symp.

Kerwin, J. E., S. A. Kinnas, J.-T. Lee and W.-Z. Shih (1987). A surface panel method for the hydrodynamic analysis of ducted propellers. Transactions of Society of Naval Architects and Marine Engineers, Presented at the Annual Meeting. New York, N.Y., November 11-14.

Krasilnikov, V. I., J. Y. Sun, Z. Zhang and F. Hong (2007). Mesh generation technique for the analysis of ducted propellers using a commercial ranse solver and its application to scale effect study. Proceedings of the 10th Numerical Towing Tank Symposium (NuTTS'07).

Lee, H. and S. A. Kinnas (2006). Prediction of cavitating performance of ducted propellers. Proc. of the 6th Int. Symp. On Cavitations.

Moon, I.-S., K.-S. Kim and C.-S. Lee (2002). Blade tip gap flow model for performance analysis of waterjet propulsors. In International Association for Boundary Element Methods, Austin, Texas, USA.

Rijpkema, D. and G. Vaz (2011). Viscous flow computations on propulsors: verification, validation and scale effects. Proc. of the Developments in Marine CFD.

Sanchez-Caja, A., P. Rautaheimo and T. Siikonen (2000). Simulation of incompressible viscous flow around a ducted propeller using a RANS equation solver. Proc. 23rd Symp. on Naval Hydrodynamics.

Sasaki, S., I. Torise and H. Hayashi (2012). An experimental and numerical study on wake vortex noise of a low speed propeller fan. Open Journal of Fluid Dynamics 2, 290-296.

Steden, M., J. Hundemer and M. Abdel-Maksoud (2009). Optimization of a linearjet, 1st Int. Symp. on Marine Propulsors (SMP'09), Trondheim, Norway.

Suryanarayana, C. h., B. Satyanarayana and K. Ramji (2014). Performance evaluation of an underwater body and pumpjet by model testing in cavitation tunnel. International Journal of Naval Architecture and Ocean Engineering 2(2), 57-67.

Takinacı, A. C. and T. Taralp (2013). Prediction and simulation of broadband propeller noise. Journal of Marine Science and Technology 21(5), 538-544.

Zondervan, G-J., M. Hoekstra and J. Holtrop (2006). Flow analysis, design and testing of ducted propellers. Proc. of Propeller/Shafting Symposium, Virginia Beach, USA.